World Academy of Science, Engineering and Technology
International Journal of Energy and Power Engineering
Vol:17, No:12, 2023

The Effect of Blockage Factor on Savonius Hydrokinetic Turbine Performance

Thochi Seb Rengma, Mahendra Kumar Gupta, P. M. V. Subbarao

***Abstract*—**Hydrokinetic turbines can be used to produce power in inaccessible villages located near rivers. The hydrokinetic turbine uses the kinetic energy of the water and maybe put it directly into the natural flow of water without dams. For off-grid power production, the Savonius-type vertical axis turbine is the easiest to design and manufacture. This proposal uses three-dimensional Computational Fluid Dynamics (CFD) simulations to measure the considerable interaction and complexity of turbine blades. Savonius hydrokinetic turbine (SHKT) performance is affected by a blockage in the river, canals, and waterways. Putting a large object in a water channel causes water obstruction and raises local free stream velocity. The blockage correction factor or velocity increment measures the impact of velocity on the performance. SHKT performance is evaluated by comparing power coefficient (C_p) with tip-speed ratio (TSR) at various blockage ratios. The maximum C_p was obtained at a TSR of 1.1 with a blockage ratio of 45%, whereas TSR of 0.8 yielded the highest C_p without blockage. The greatest C_p of 0.29 was obtained with a 45% blockage ratio compared to a C_p max of 0.18 without a blockage.

***Keywords*—**Savonius hydrokinetic turbine, blockage ratio, vertical axis turbine, power coefficient.

I. Introduction

BOTH social scientists and scientific community are expressing great concern over the escalating environmental challenges through proper employment of the viable natural renewable energy sources [1]. Affirmatively, special attention is given by the government to harness such power sources in order to palliate carbon emissions from coal-based energy plants [2]. This milieu brought to light the desirable alternative of hydroelectric energy except its certain macroscale projects-related objections of higher demanding expenditure and substantial environmental unfriendliness. Researches have shown unexpected high methane emission in reservoir basin projects, thereby, raising dubiety on the seemingly carbon-friendly slant inconclusively [3]. These hindrances brought friction in further accruing exploration of the future of the country's hydroelectric energy.

While maintaining comparatively lower carbon emissions, rural absorption of microscale and contextualized pico-hydel or hydrokinetic turbines ensures electrification in far-flung and inaccessible sites. Such turbines can be manufactured to produce power by maintaining low cost and efficient maintenance in an ideal water flowing velocities of 1.0-2.0 m/s. Hydrokinetic turbines are usually categorized as vertical axis hydrokinetic turbine (VAHT) and horizontal axis hydrokinetic turbine (HAHT) [4]. While the latter provides better power co-efficiency [5], [6] the former is applied mostly in the rivers and canals owing to its simplicity and cost-effective technology [7]. The simple and easily installable turbine is [8] SHKT which is a VAHT type, which was first created in 1920s by Savonius. Fig. 1 depicts the schematic depiction of its working principle. Its traditional model is constructed by slicing a cylinder centrally in an S-shaped cross-section conformation [9]. SHKT is depicted with detailed geometric parameters in Fig. 2.

Fig. 1 The working principle of the SHKT system

As shown in Fig. 2, the drag force between advancing and returning blades is deducible that controls the turbine rotation. The net driving force depends on exerted force of either increase on the advancing or decrease on the returning blades [10]. The desirable resulting varying co-efficiency of drag is produced due to the spinning of the turbine on its own axis based on unilateral flow of water, ultimately, bringing a rotor-induced change in torque [11]. This transitional process of the rotor occurs in cyclical fluctuations [12]. The resultant mechanical energy conversion occurs due to transformation of kinetic energy of a moving river current of hydrokinetic turbines. This type of turbine is also often referred to as ultra-low head and zero water turbines [4]. It provides advantages of effortless fabrication, minimal noise, better self-starting and reduced wear of moving parts [13]-[16].

The influence of wall effect on the turbine performance was studied by varying the blockage ratio. A study by Takeda and Kato [29] revealed that in the test with a blockage ratio of less than 5%, there are no major blockage effects. Modi et al. [27], [28] did not provide any details of blockage correction but positively stated that an increase in wall confinement from 5% to 20% can raise the power coefficient by around 70%. This can lead to a highly inaccurate performance estimate if the blockage

Thochi Seb Rengma*, Mahendra Kumar Gupta, and P.M.V. Subbarao are with Department of Mechanical Engineering, Indian Institute of Technology Delhi, India (*Corresponding author, e-mail: thochirengma@gmail.com

correction is not done. Tests conducted by Jeong et al. [30] proved that any wind tunnel test that has a blockage ratio higher than 10% must undergo a correction method. The magnitude of the blockage effect on the drag coefficient was even significant at 5% of the blockage ratio. When the blockage ratio is increased, the absolute value of backpressure is found to increase. This directly caused the increase in the drag coefficient.

TABLE I
NOMENCLATURE OF PARAMETERS

H	Height of turbine [m]	W	Weight of water channel
D	Diameter of turbine [m]	ρ	Density of water [kg/m^3]
D_o	Diameter of end plate [m]	P	Power [W]
θ	Rotational angle [degree]	C_P	Power coefficient
e	Gap between the two blades [m]	$C_{P\,max}$	Maximum power coefficient
t	Thickness of the blades [m]	C_m	Moment coefficient
A	Area (H×D) [m^2]		Abbreviations
U	Free stream velocity [m/s]	BR	Blockage ratio (HD/H_wW)
g	Gravitational acceleration [m/s^2]	AR	Aspect ratio [H/D]
ω	Angular velocity [rad/s]	OR	Overlap ratio [e/D]
H_w	Height of the water channel	TSR	Tip speed ratio [ωD/2U]

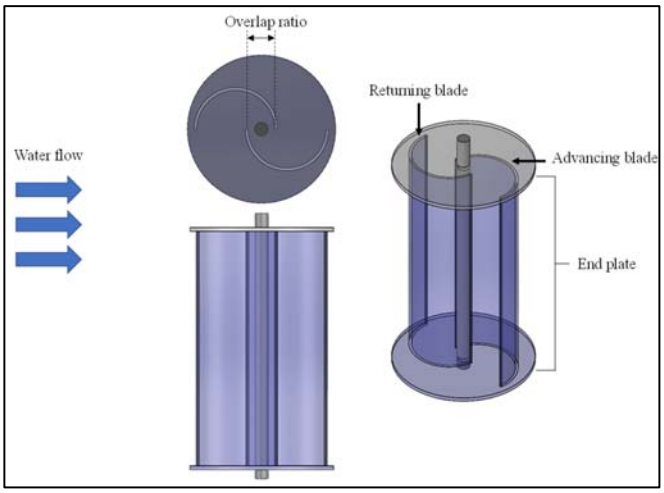

Fig. 2 Schematic diagram of SHKT

Two-bladed Savonius turbines are considered for the analysis as it shows better performance [17]. The aspect ratio of 1.8 and overlap ration of 0.15 are found to be more efficient as stated by the author in the previous publication [18].

II. Data Reduction

The actual power captured by the turbine is given as:

$$P_{Turbine} = C_P \frac{1}{2} \rho A U^3 \quad (1)$$

The power coefficient of hydrokinetic turbines depends on the TSR, which is defined as the ratio of the blade speed at the tip to the speed of the water [19]. The expression of TSR is given as:

$$\lambda = \frac{\omega D}{2U} \quad (2)$$

Blockage ratio (BR) is the ratio of the model area to the test section of the water channel. The BR is given as:

$$BR = \frac{HD}{H_w W} \quad (3)$$

The torque coefficient (C_m) is generally expressed as:

$$C_m = \frac{T}{\frac{1}{2}\rho A U^2 R} \quad (4)$$

The power coefficient (Cp) is defined as the ratio of power output and power input. The expression of C_p is given as:

$$C_p = C_m \lambda \quad (5)$$

III. Computational Methodology

The optimization of blockage ratio is analyzed using computational modeling. A fluid is considered to be incompressible, which follows unsteady flow behavior, and turbulent viscosity was supposed to be isotropic, meaning Reynolds stress and mean deformation rate are the same in all directions. Thermal radiation is ignored, and walls are adiabatic.

A. Computational Domain and Boundary Conditions

The blade shape and geometry were designed in SolidWorks. The geometry was then imported to ANSYS design modeler to create the three-dimensional geometry domain based on parameters in Table II. To capture the turbine's rotational movement, a cylinder casing was created around it. Two zones were created in the 3D computational fluid domain (i.e., rotating zone and stationary zone). The rotating zone was used to model the rotational behavior of the turbine near the blades. To keep the flow continuous, the cylinder's circumference was set as an interface. The length, width and height of the computational domain were kept as 4.5 m, 1.2 m and 1.2 m, respectively. The turbine was placed at 1.5 m distance from the inlet plane. The enclosure of the rotating cylinder was taken as 1.5 D. The open channel computational domain in 3D is depicted in Fig. 4.

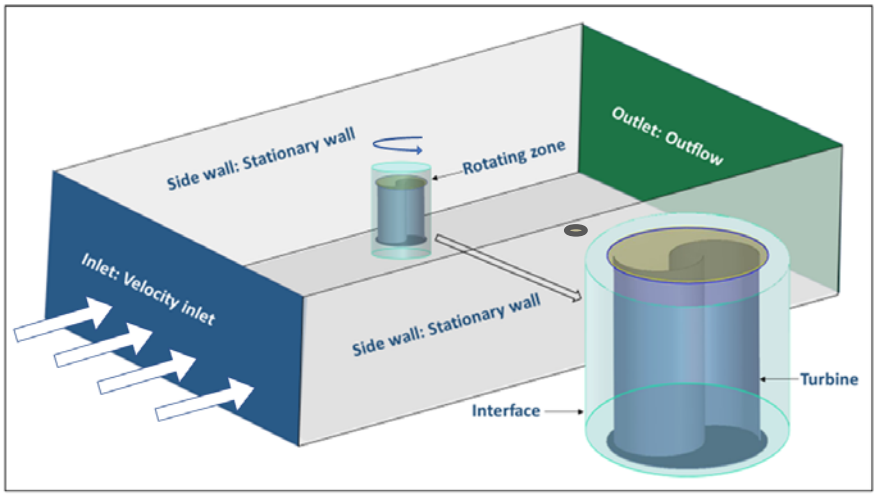

Fig. 4 3D computational domain of open channel

TABLE II
GEOMETRIC PARAMETER OF MODIFIED SHKT

Parameter	value
Aspect ratio (H/D)	1.8
Overlap ratio (e)	0.2
Blade diameter (D)	250 mm
Blade height (H)	450 mm
Endplate diameter (D_0)	275 mm
Blade arc angle (Φ)	100° to 200° (20° per interval)
Blade shape factor (p/q)	0 to 1 (0.2 per interval)
Blade thickness	2 mm

In this investigation, the rotational dynamics of the inner domain were addressed through the application of a steady-state solver employing a Multiple Reference Frame (MRF). Subsequently, the solution underwent a transition to a transient state, facilitated by the utilization of a Sliding Mesh Motion (SMM) technique. The convergent steady-state outcome from the MRF simulation served as the initial condition for the transient SMM solver.

The transient flow problem was tackled using a Finite Volume Method (FVM) coupled with MRF, specifically applied to a rotating zone characterized by a defined angular velocity. Convective term discretization was executed using a second-order upwind scheme, and pressure interpolation was achieved through a linear interpolation scheme.

For each time step, the convergence criterion for continuity was established, targeting a residual value of 10^{-5}.

The determination of the time step size was contingent upon the angular velocity (RPM) of the shaft, with a calculated time step for every 5° of turbine rotation. The simulation spanned six complete rotations, with a maximum of 500 iterations allowed per time step. Table III provides the boundary conditions of a numerical analysis. The continuity equation and Navier Stokes equations were solved using Semi-Implicit Methods for Pressure-Linked Equations (SIMPLE). SIMPLE is an algorithm to discretize the momentum equation and pressure correction implicitly and the velocity correction equation explicitly. The under-relaxation factors for pressure and momentum were set as 0.4 and 0.5, respectively.

TABLE III
BOUNDARY CONDITION OF NUMERICAL SIMULATIONS

Name	Boundary conditions
Inlet	Velocity inlet
Outlet	Outflow
Channel top surface	Symmetry
Side and bottom wall	No slip wall
Rotating zone	MRF
Turbine	No slip

B. Mesh Generation and Validation of Computational Model

As illustrated in Fig. 5, a non-conformal unstructured grid size with tetrahedral elements was employed for meshing. This is because tetrahedral elements are less costly, can fit a complex geometry better and are capable of providing local body mesh refinements. The mesh was refined in the inner domain areas as large gradients of flow were expected and coarse mesh was selected for the outer domain. To capture the flow physics near the turbine blades, 10 inflating layers, with first layer height of 0.07 mm, were produced near the blades to maintain the y+ value ~1.

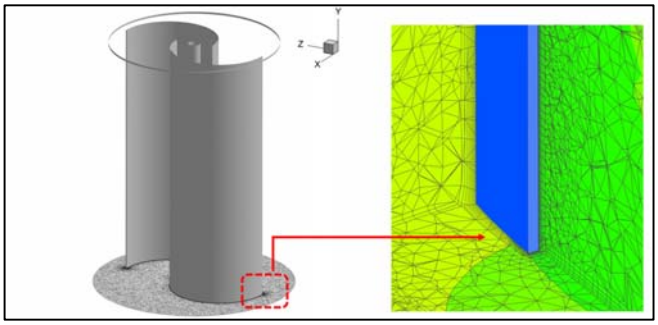

Fig. 5 Meshing of the blade in model channel

To confirm the current computational analysis with the reported experimental result at Reynolds number 1.35×10^5 [20], several turbulence models were evaluated against altering TSR.

The Realizable k-ϵ model (Enhance wall fn.) was observed to follow the same trend as the experimental data of T. Hayashi et al. [20]. With rising TSR, the value of the moment coefficient dropped. The difference between experimental and computed data was less than 10%. Thus, realizable k-ϵ model was chosen for this investigation because it better simulated the rotating behavior of blades and flow through the channel which was also stated by other researchers [21]-[23]. This model includes turbulent viscosity and a new dissipation rate transport equation. The published experimental model was used to validate the turbulence model, and the realizable k-ϵ model (enhance wall function) exhibited good agreement with the published experimental results [20], as shown in Fig. 6.

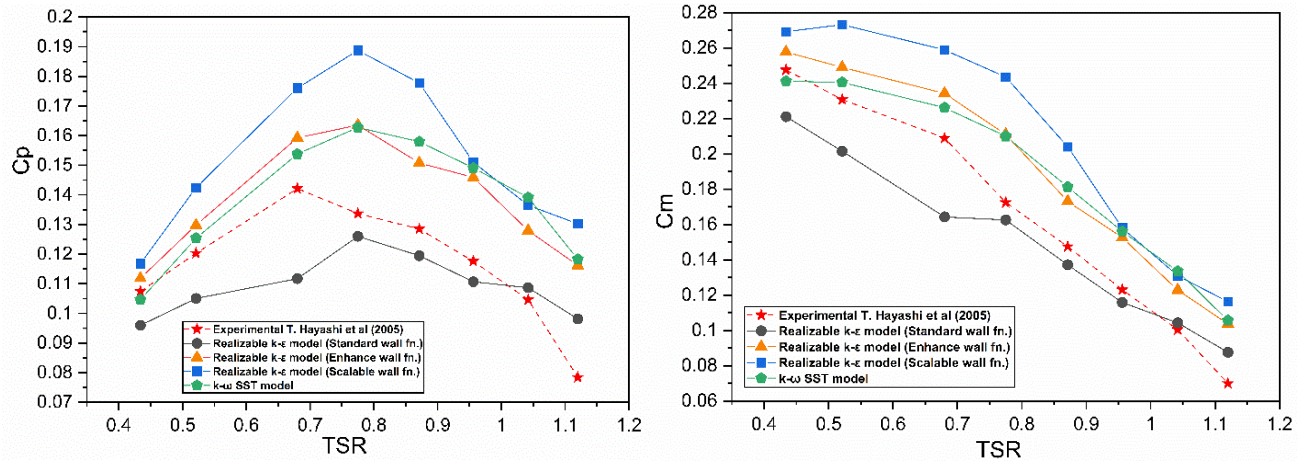

(a) (b)

Fig. 6 Validation of turbulence model (a) Power coefficient (b) Torque coefficient, compared to publish experimental results

IV. Results and Discussion

SHKT performance is affected by blockage in the river, canals, and waterways. Putting a large object in a water channel causes water obstruction and raises local free stream velocity. Blockage correction factor or velocity increment measures the impact of velocity on the performance [24]. Detailed study on evaluating this effect has been observed in the literature [25]. SHKT performance is evaluated by comparing power coefficient (C_p) with TSR at various blockage ratios. The C_p against TSR was plotted for a range of 0% overlap to 45% overlap to understand the holistic effect of blockage on the turbine performance.

The comparative plot from Fig. 7 provides evidence of a rightward shift in efficiency peak when the blockage ratio is increased by decreasing the size of the channel domain. This happens because when a larger body placed within the flow, it leads to a higher level of flow constriction, thus enhancing the freestream velocity. It clearly shows a dramatic increase in power coefficient which was also reported by Alexander [26] and Modi et al. [27], [28].

Fig. 7 shows the distribution of power coefficient and torque coefficient at different TSR for blockages ratio of 0%, 5%, 11.25%, 17.57%, 22.95%, 31.25% and 45% at a Reynolds number of 100,000. Power coefficient almost remained constant for blockage ratios 0%, 5%, and 11.25%. The maximum coefficient of power occurred at a TSR in the range of 0.8 to 1.2. The maximum coefficient of static torque increased marginally with an increase in the blockage ratio from 11.25% to 17.57%. The highest C_p with blockage ratio 45% was achieved at TSR value of 1.1, whereas the $C_{p\ max}$ without blockage was observed at TSR 0.8. With increase in the blockage ratio, the value of $C_{p\ max}$ corresponding to TSR also shifted towards right. The highest C_p with blockage ratio of 45% was found to be 0.29, compared to $C_{p\ max}$ of 0.18 without blockage. The fluctuation of moment coefficient with respect to azimuth angle is shown in Fig. 8 (a) and the polar coordinates of turbine rotation of one complete circle is given in Fig. 8 (b).

V. Conclusion

This study investigated the optimization of blade profile of SHKT using computational analysis. It includes the study the wall effect on the turbine performance. The power coefficient (C_p) and moment coefficient (C_m) of the turbine corresponding to different TSRs value are calculated by varying a blockage ratio. The results can be summarized as follows:

i. The maximum C_p was obtained at TSR of 1.1 with blockage ratio of 45%, whereas TSR 0.8 yielded the highest C_p without blockage.
ii. The greatest C_p of 0.29 was obtained with a 45% blockage ratio compared to a C_p max of 0.18 without a blockage.

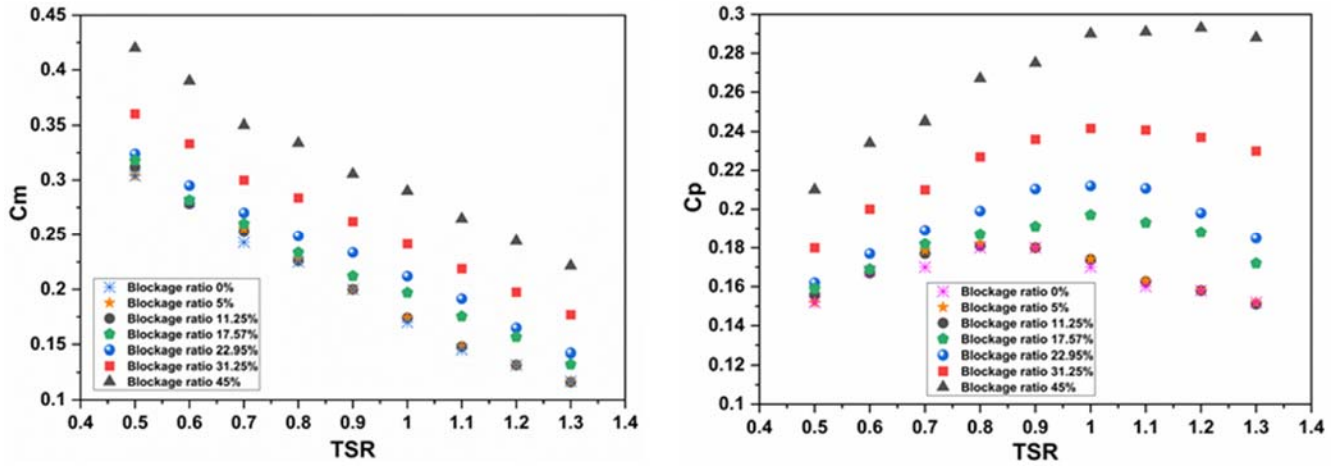

(a) (b)

Fig. 7 (a) C_m vs. TSR (b) C_p vs. TSR

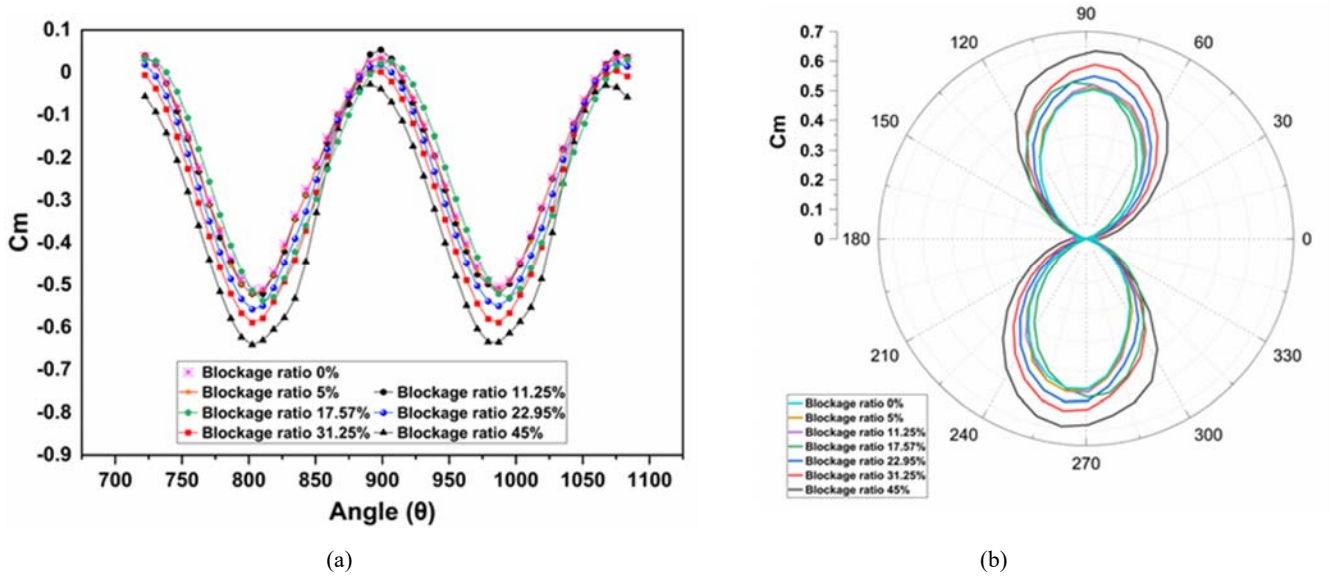

(a) (b)

Fig. 8 Cm vs. rotation of blade angle (θ)

REFERENCES

[1] J. A. Duffie and W. A. Beckman, *Solar Engineering of Thermal Processes: Fourth Edition*. 2013.

[2] M. Ghasemian, Z. N. Ashrafi, and A. Sedaghat, "A review on computational fluid dynamic simulation techniques for Darrieus vertical axis wind turbines," *Energy Convers. Manag.*, vol. 149, pp. 87–100, 2017, doi: 10.1016/j.enconman.2017.07.016.

[3] O. Paish, "Small hydro power: Technology and current status," *Renew. Sustain. Energy Rev.*, vol. 6, no. 6, pp. 537–556, 2002, doi: 10.1016/S1364-0321(02)00006-0.

[4] M. J. Khan, G. Bhuyan, M. T. Iqbal, and J. E. Quaicoe, "Hydrokinetic energy conversion systems and assessment of horizontal and vertical axis turbines for river and tidal applications: A technology status review," *Appl. Energy*, vol. 86, no. 10, pp. 1823–1835, 2009, doi: 10.1016/j.apenergy.2009.02.017.

[5] A. De Marco, D. P. Coiro, D. Cucco, and F. Nicolosi, "A numerical study on a vertical-axis wind turbine with inclined arms," *Int. J. Aerosp. Eng.*, vol. 2014, 2014, doi: 10.1155/2014/180498.

[6] M. K. Gupta and P. M. V. Subbarao, "Development of a semi-analytical model to select a suitable airfoil section for blades of horizontal axis hydrokinetic turbine," *Energy Reports*, vol. 6, no. February, pp. 32–37, 2020, doi: 10.1016/j.egyr.2019.08.014.

[7] M. Badrul Salleh, N. M. Kamaruddin, and Z. Mohamed-Kassim, "Savonius hydrokinetic turbines for a sustainable river-based energy extraction: A review of the technology and potential applications in Malaysia," *Sustain. Energy Technol. Assessments*, vol. 36, no. July, p. 100554, 2019, doi: 10.1016/j.seta.2019.100554.

[8] T. S. Rengma, A. R. Sengupta, M. Basumatary, A. Biswas, and D. Bhanja, "Performance analysis of a two bladed Savonius water turbine cluster for perennial river-stream application at low water speeds," *J. Brazilian Soc. Mech. Sci. Eng.*, vol. 43, no. 5, 2021, doi: 10.1007/s40430-021-02982-x.

[9] S. Savonius, "The S-rotor and its applications," *Mech. Eng.*, vol. 53, no. 5, pp. 333-338., 1931.

[10] M. A. Kamoji, S. B. Kedare, and S. V. Prabhu, "Experimental investigations on single stage, two stage and three stage conventional Savonius rotor," *Int. J. energy Res.*, vol. 32, no. 2008, pp. 877–895, 2008, doi: 10.1002/er.

[11] T. S. Rengma and P. M. V. Subbarao, "Comparative Analysis of Savonius Type Ultra-Micro Hydrokinetic Turbine of Experimental and Computational Investigation," p. 380, 2022, Online. Available: 10.1007/978-981-16-3497-0_19.

[12] S. Bhuyan and A. Biswas, "Investigations on self-starting and performance characteristics of simple H and hybrid H-Savonius vertical

axis wind rotors," *Energy Convers. Manag.*, vol. 87, pp. 859–867, 2014, doi: 10.1016/j.enconman.2014.07.056.

[13] R. Gupta, A. Biswas, and K. K. Sharma, "Comparative study of a three-bucket Savonius rotor with a combined three-bucket Savonius-three-bladed Darrieus rotor," *Renew. Energy*, vol. 33, no. 9, pp. 1974–1981, 2008, doi: 10.1016/j.renene.2007.12.008.

[14] A. Bianchini, F. Balduzzi, P. Bachant, G. Ferrara, and L. Ferrari, "Effectiveness of two-dimensional CFD simulations for Darrieus VAWTs: a combined numerical and experimental assessment," *Energy Convers. Manag.*, vol. 136, pp. 318–328, 2017, doi: 10.1016/j.enconman.2017.01.026.

[15] N. H. Abu-Hamdeh and K. H. Almitani, "Construction and numerical analysis of a collapsible vertical axis wind turbine," *Energy Convers. Manag.*, vol. 151, no. June, pp. 400–413, 2017, doi: 10.1016/j.enconman.2017.09.015.

[16] K. Golecha, T. I. Eldho, and S. V. Prabhu, "Study on the interaction between two hydrokinetic Savonius turbines," *Int. J. Rotating Mach.*, vol. 2012, 2012, doi: 10.1155/2012/581658.

[17] L. Chen, J. Chen, H. Xu, H. Yang, C. Ye, and D. Liu, "Wind tunnel investigation on the two- and three-blade Savonius rotor with central shaft at different gap ratio," *J. Renew. Sustain. Energy*, vol. 8, no. 1, 2016, doi: 10.1063/1.4940434.

[18] T. S. Rengma and P. M. V. Subbarao, "Optimization of semicircular blade profile of Savonius hydrokinetic turbine using artificial neural network," *Renew. Energy*, 2022, Online. Available: https://doi.org/10.1016/j.renene.2022.10.021.

[19] B. Jones, *Elements of aerodynamics*. New York: J. Wiley, 1889.

[20] T. Hayashi, Y. Li, and Y. Hara, "Wind Tunnel Tests on a Different Phase Three-Stage," vol. 48, no. 1, pp. 9–16, 2005.

[21] M. H. Mohamed, G. Janiga, E. Pap, and D. Thévenin, "Optimal blade shape of a modified Savonius turbine using an obstacle shielding the returning blade," *Energy Convers. Manag.*, vol. 52, no. 1, pp. 236–242, 2011, doi: 10.1016/j.enconman.2010.06.070.

[22] M. R. Castelli and E. Benini, "Effect of blade inclination angle on a Darrieus wind turbine," *J. Turbomach.*, vol. 134, no. 3, pp. 1–10, 2011, doi: 10.1115/1.4003212.

[23] Y. Chen and Y. Lian, "Numerical investigation of vortex dynamics in an H-rotor vertical axis wind turbine," *Eng. Appl. Comput. Fluid Mech.*, vol. 9, no. 1, pp. 21–32, 2015, doi: 10.1080/19942060.2015.1004790.

[24] K. Morshed, M. Rahman, G. Molina, and M. Ahmed, "Wind tunnel testing and numerical simulation on aerodynamic performance of a three-bladed Savonius wind turbine," *Int. J. Energy Environ. Eng.*, vol. 4, no. 1, p. 18, 2013, doi: 10.1186/2251-6832-4-18.

[25] R. E. Sheldahl, B. F. Blackwell, and L. V. Feltz, "Wind Tunnel Performance Data for Two- and Three-Bucket Savonius Rotors.," *J Energy*, vol. 2, no. 3, pp. 160–164, 1978, doi: 10.2514/3.47966.

[26] A. J. Alexander and B. P. Holownia, "Wind Tunnel Tests on a Savonius Rotor," *J. Ind. Aerodyn.*, vol. 3, no. 4, pp. 343–351, 1978, doi: 10.1016/0167-6105(78)90037-5.

[27] V. J. Modi and M. S. U. K. Fernando, "On the performance of the savonius wind turbine," *J. Sol. Energy Eng. Trans. ASME*, vol. 111, no. 1, pp. 71–81, 1989, doi: 10.1115/1.3268289.

[28] V. J. Modi, N. J. Roth, and M. S. U. K. Fernando, "Optimum-configuration studies and prototype design of a wind-energy-operated irrigation system," *J. Wind Eng. Ind. Aerodyn.*, vol. 16, no. 1, pp. 85–96, 1984, doi: 10.1016/0167-6105(84)90050-3.

[29] K. Takeda and M. Kato, "Wind tunnel blockage effects on drag coefficient and wind-induced vibration," *J. Wind Eng. Ind. Aerodyn.*, vol. 41–44, pp. 897–908, 1992.

[30] H. Jeong, S. Lee, and S. D. Kwon, "Blockage corrections for wind tunnel tests conducted on a Darrieus wind turbine," *J. Wind Eng. Ind. Aerodyn.*, vol. 179, no. June, pp. 229–239, 2018, doi: 10.1016/j.jweia.2018.06.002.